

Statistical Shape Modeling of Musculoskeletal Structures and Its Applications

Hans Lamecker^{1,2}, Stefan Zachow¹

¹ Zuse Institute Berlin (ZIB), Takustr. 7, 14195 Berlin, Germany

² 1000shapes GmbH, Wiesenweg 10, 12247 Berlin, Germany

December 15, 2015

Contents

1	Introduction	1
2	Statistical Shape Modeling	2
2.1	Representation	2
2.2	Comparison	3
2.3	Statistical Analysis	4
2.4	Evaluation	5
3	Applications	6
3.1	Anatomy Reconstruction	6
3.1.1	Example: Knee-Joint Reconstruction from MRI	8
3.1.2	Example: 3D reconstruction from X-ray	12
3.2	Reconstructive Surgery	16
3.2.1	Example: Mandible dyplasia	17
3.2.2	Example: Craniosynostosis	18
3.2.3	Example: Surgical Reconstruction of Complex Fractures in the Midface	20
3.3	Population-based Analysis	23
3.3.1	Example: A large scale finite element study of total knee replacements	23
3.3.2	Example: Digital Morphometry of Facial Anatomy, From Global to Local Shape Variations	25
4	Conclusions	29

Abstract

Statistical shape models (SSM) describe the shape variability contained in a given population. They are able to describe large populations of complex shapes with few degrees of freedom. This makes them a useful tool for a variety of tasks that arise in computer-aided medicine. In this chapter we are going to explain the basic methodology of SSMs and present a variety of examples, where SSM has been successfully applied.

1 Introduction

The morphology of anatomical structures plays an important role in medicine. Not only does the shape of organs, tissues and bones determine the aesthetic appearance of the human body, but it is also strongly intertwined with its physiology. A prominent example is the musculoskeletal system, where the shape of bones is an integral component in understanding the complex biomechanical behavior of the human body. Such understanding is the key to improving therapeutic approaches, e.g. for treating congenital diseases, traumata, degenerative phenomena like osteoporosis, or cancer.

With the advent of modern imaging systems like X-ray computed-tomography (CT), magnetic resonance imaging (MRI), three-dimensional (3D) ultrasound (US) or 3D photogrammetry a variety of methods is available both for capturing the 3D shape of anatomical structures inside or on the surface of the body. This has opened up the opportunity of more detailed diagnosis, planning as well as intervention on a patient-specific basis. In order to transfer such developments into clinical routine and facilitate access for every patient in a cost-effective way, efficient and reliable methods for processing and analyzing shape data are called for.

In this chapter, we are going to turn the attention on a methodology, which shows great promises for efficient and reliable processing and analysis of 3D shape data in the context of orthopedic applications. We are going to describe the conceptual framework as well as illustrate the potential impact to improving health care with selected examples from different applications.

This chapter is not intended to give an exhaustive overview over the work done in field of statistical shape modeling. Instead, it shall serve as an introduction to the technology and its applications, with the hope that the reader is inspired to convey the presented ideas to his field of

work.

2 Statistical Shape Modeling

In this section, the basic conceptual framework of statistical shape modeling is described. There is a large variety of different approaches to many aspects of statistical shape modeling, such as shape representation or comparison techniques, which shall not be covered here. Instead, we are focusing on extracting the essential links and facts in order to understand the power of statistical shape modeling in the context of the applications. The reader interested in more details is referred to [16]. An overview specific to bone anatomy is presented by Sarkalkan et al. [19].

2.1 Representation

3D shape describes the external boundary form (surface) of an object, independent of its location in space. The size of an object hence is part of its shape. For the scope of this chapter, it suffices to know that mathematically, a surface S is represented by a – in general infinite – number of parameters and/or functions x , which describe the embedding of the surface in space, and thus its form. The computerized digital surface representation $S(x)$ in general approximates the shape by reducing the infinite number of parameters x to a finite set. One commonly used representation in computer graphics are triangle meshes, which are point clouds, where the points are connected by triangles, but many other representations like skeletons, splines, etc. are also used.

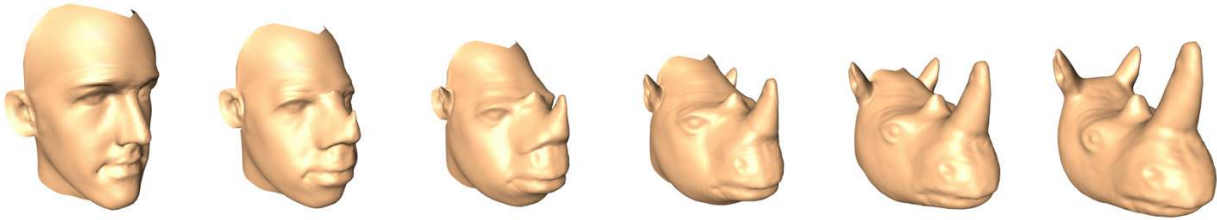


Figure 1: Transformation of a human into a rhinoceros head is made possible through the representation of shapes in a common shape space.

2.2 Comparison

The fundamental task to analyze shapes is to compare two shapes S_1 and S_2 . This means that for each parameter x_1 for shape S_1 a corresponding parameter x_2 for shape S_2 is identified. One important prerequisite is that such an identification method needs to be independent of the location of the two shapes in 3D space. Such a process is also referred to as matching or registration. For example, for each 3D point on one surface a corresponding 3D point on the other surface may be identified. For other representations, these may not be 3D points but e.g. skeletal parameters, etc. As a consequence one can establish a so-called shape space, where shapes may be treated just like numbers in order to perform calculations on shapes, like e.g. averaging $S_3 = 0.5 \cdot (S_1 + S_2)$ or any other interpolation, see Fig. 1.

It is obvious that the details of the correspondence identification has great impact on subsequent analysis, see Fig. 2. Nevertheless, a proper definition for “good” correspondences is difficult to establish in general, and in most cases must be provided in the context of the application. One generic approach to establish correspondence, however, optimizes the resulting statistical shape model built from the correspondences, i.e. its compactness of generalization ability, see Sec. 2.4. Refer to Davies et al. [3] for more details.

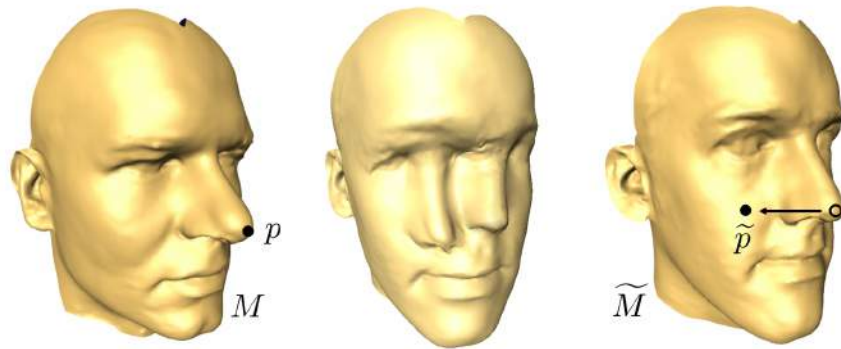


Figure 2: When the tip of the nose on the left head is matched with a point on the cheek on the right head, shape interpolation may yield a head with two noses.

2.3 Statistical Analysis

As soon as we are able to perform “shape arithmetic” in a shape space, we can perform any kind of statistical analysis, e.g. like principal component analysis (PCA). This kind of analysis takes as input a set of training shapes S_1, \dots, S_n and extracts the so-called modes of variations V_1, \dots, V_{n-1} sorted by their variance in the training set. Together with the mean shape \bar{S} the modes of variations form a statistical shape model (SSM):

$$S(b_1, \dots, b_{n-1}) = \bar{S} + \sum_{k=1}^{n-1} b_k \cdot V_k \quad (1)$$

The SSM is a family of shapes determined by the parameters b_1, \dots, b_{n-1} , each of which weights one of the modes of variations V_k . For instance, if we set $b_2 = \dots = b_{n-1} = 0$ and vary only b_1 we will see the effect of the first mode of variation on the deformations of the shapes within the range of the training population. The PCA may be exchanged with other methods, which will alter the interpretation of both the V_k and their weights b_k . See Sec. 3.3.2 for such an alternative approach.

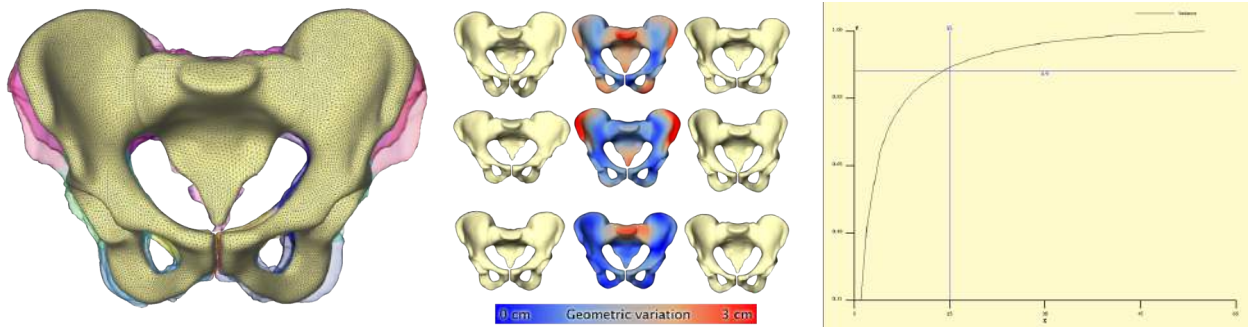


Figure 3: Left: Overlay of several training shapes. Middle: First three modes of variation from top to bottom. Local deformation strength is color-coded. Right: 90 percent variation within 15 shape modes.

In the PCA case, the idea is that the variance within the training population is contained in only few modes, hence the whole family of shapes can be described with only a few “essential degrees of freedom”, see Fig. 3. Note that the shape variations V_i are generally global deformations of the shape, i.e. they vary every point on the shape. Thus, a SSM can be highly compact representation of a family of complex geometric shapes. Furthermore, it is straightforward to synthesize new shapes by choosing new weights. These may lie within the range of the training shapes or even extrapolate beyond that range.

2.4 Evaluation

With the SSM we can represent any shape as a linear combination of the input shapes or some kind of transformation of those input shapes, e.g. via PCA. However, up to what accuracy can we represent/reconstruct an unknown shape S^* by an SSM $S(b)$? The idea is to compute the best approximation of the SSM to the unknown shape:

$$b^* = \operatorname{argmin}_b d(S^*, S(b)) \quad (2)$$

where $d(\cdot, \cdot)$ is a measure for the distance between two shapes. Then $S(b^*)$ is the best approximation of S^* within the SSM.

If $d(S^*, S(b^*)) = 0$ then the unknown shape is already “contained” in the SSM, otherwise the SSM is not capable of explaining S^* . The smaller $d(S^*, S(b^*))$ for any S^* , the higher the so-called generalization of the SSM. A better generalizability can be achieved by including more training samples into the model generation process. A good SSM has a high generalization or reconstruction capability. On the other hand, if $S(b)$ for an arbitrary b is similar to any of the training data sets S_1, \dots, S_n , the SSM is said to be of high specificity. In other words, synthesized shapes do indeed resemble real members of the training population. Generalization and specificity need to be verified experimentally.

3 Applications

3.1 Anatomy Reconstruction

One of the basic challenge in processing medical image data is the automation of segmentation or anatomy reconstruction. Due to noise, artifacts, low contrast, partial field-of-view and other measurement-related issues, the automatic delineation and discrimination of specific structures from other structures or the background – seemingly an easy task for the human brain – is still challenging for the computer.

However, over the last two decades, model-based approaches have shown to be effective to tackle this challenge, at least for well-defined application-specific settings. The basis idea is the use a deformable shape template (such as a SSM) and match it to medical image data like CT

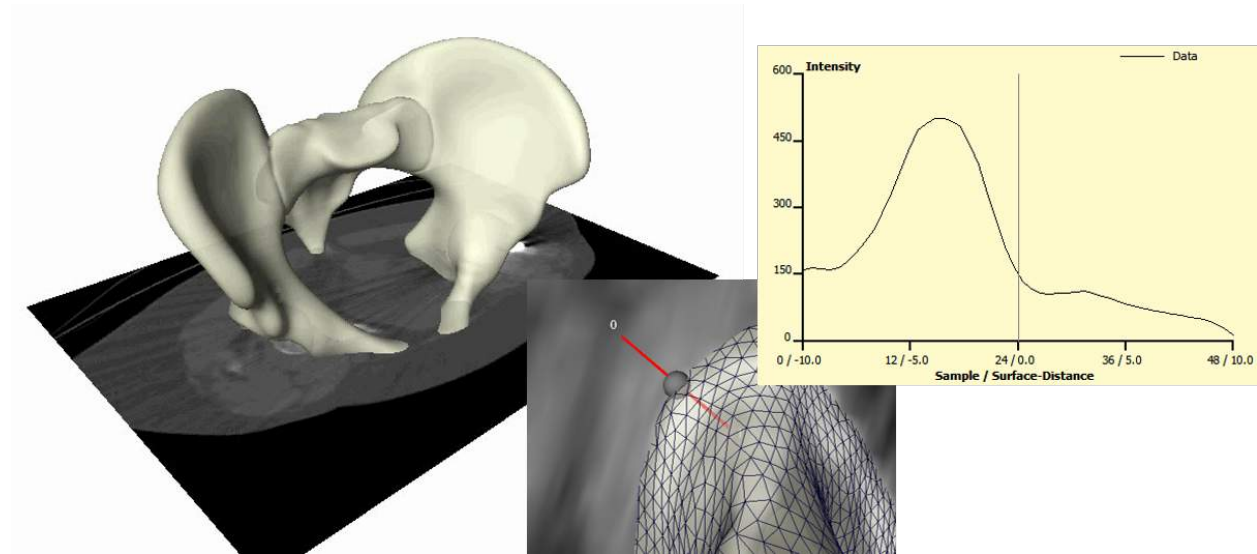


Figure 4: A SSM is matched to CT data. At each point of the surface an intensity models predicts the desired deformation.

or MRI. In this case, the shape S^* from equation (2) is not known explicitly. Therefore, such an approach – in addition to the SSM – requires a intensity model, that quantifies how well an instance of the SSM fits to the image data, see Fig. 4. From such a model, S^* can be estimated. Many such intensity models have been proposed in the literature. One generic approach is to “learn” such a model from training images similar to the way SSMs are generated [2]. Shape models are also combined with intensity models in SSIMs or shape and appearance Models. An overview can be found in [10].

The strength of this approach is its robustness stemming from the SSM. Only SSM instances can be reconstructed, thus this method can successfully cope with noisy, partial, low-dimensional or sparse image data.

On the other hand, since the SSM is generally limited in its generalization capability, some additional degrees of freedom are often required in order to get a more accurate reconstruction. Here,

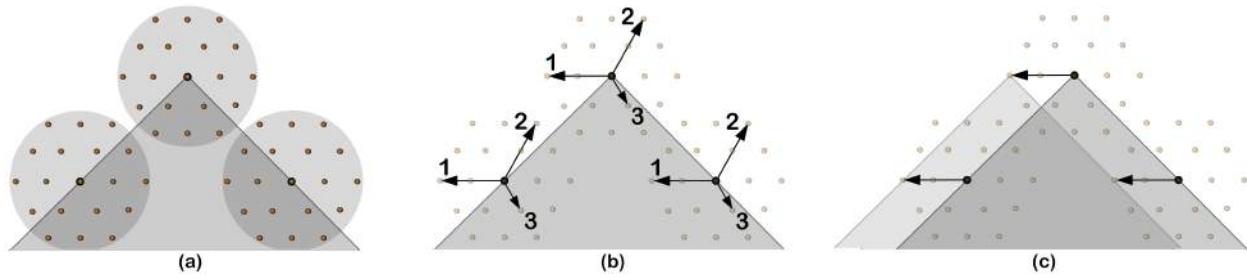


Figure 5: Instead of just normal displacements as show in Fig. 4, omnidirectional displacements allow for much more flexibility of local deformations, e.g. in regions of high curvature consistent local translations can be modeled.

finding a trade-off between robustness and accuracy remains an issue. One successful approach for achieving such a trade-off are so called omni-directional displacements [13], see Fig. 5.

3.1.1 Example: Knee-Joint Reconstruction from MRI

Osteoarthritis (OA) is a disabling disease affecting more than one third of the population over the age of 60. Monitoring the progression of OA or the response to structure modifying drugs requires exact quantification of the knee cartilage by measuring e.g. the bone interface, the cartilage thickness or the cartilage volume. Manual delineation for detailed assessment of knee bones and cartilage morphology, as it is often performed in clinical routine, is generally irreproducible and labor intensive with reconstruction times up to several hours.

Seim et al. [20] present a method for fully automatic segmentation of the bones and cartilages of the human knee from MRI data. Based on statistical shape models and graph-based optimization, first the femoral and tibial bone surfaces are reconstructed. Starting from the bone surfaces the cartilages are segmented simultaneously with a multi-object technique using prior knowledge on the variation of cartilage thickness.

For evaluation, 40 additional clinical MRI datasets acquired before knee replacement are available. A detailed evaluation is presented in Fig. 7. For tibial and femoral bones the average (AvgD) and the roots mean square (RMS) surface distances were computed. Cartilage segmentation is quantified by volumetric overlap (VOE) and volumetric difference (VD) measures. For all four structures a score was computed indicating the agreement with human inter-observer variability. Reaching the inter-observer variability results in 75 points, while obtaining an exact match to one distinguished manual segmentation results in 100 points. An error twice as high as the human rater's gets 50 points, 3x as high gets 25 points and if 4x as high or more receives 0 points (no negative points). All points are averaged for each image, which results in a total score per image. Details on the evaluation procedure are published in an overview article of the Grand Challenge workshop (www.grand-challenge.org). The average performance of our auto-segmentation system for knee bones and associated cartilage was 64.4 ± 7.5 points. Exemplary results are shown in Fig. 6.

The bone segmentation achieves scores that indicate an error larger than that obtained by human experts. This may be due to relatively large mismatches of the SSM at the proximal and distal end of the MRI data due to missing or weak image features related to intensity inhomogeneities stemming from the MRI sequence (see Fig. 8). A strong artifact of unknown source (see Fig. 8) lead to the worst segmentation result for the tibia. The scores for cartilage segmentation are based on different error measures (volumetric) and are generally better, presumably due to a higher inter-observer variability.

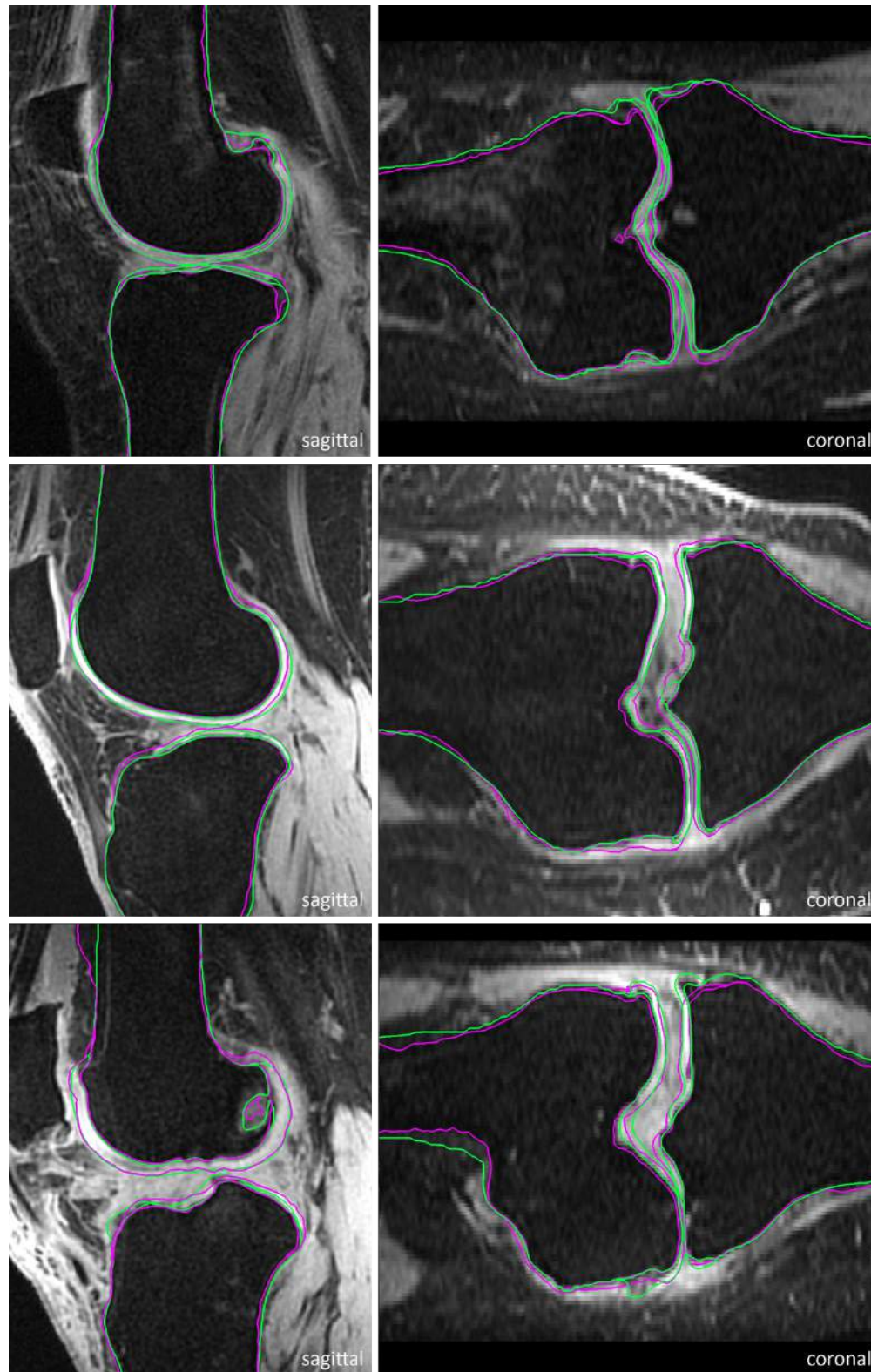


Figure 6: Selected test cases sorted by quality in terms of achieved score. Top to bottom: bad case, medium case, and good case. Pink: Automatic segmentation. Green: Ground truth.

Image	Femur		Tibia		Fem. Cartilage		Tibial Cartilage		Total Score
	AvgD [mm]	RMS [mm]	AvgD [mm]	RMS [mm]	VOE [%]	VD [%]	VOE [%]	VD [%]	
1	0,61	1,15	0,70	1,38	39,3	24,4	45,0	69,3	49
2	0,69	1,17	0,49	0,80	27,3	11,7	12,7	5,5	73
3	0,56	0,87	0,45	0,73	27,3	-14,3	23,5	8,5	71
4	0,73	1,24	0,57	0,83	35,5	31,3	30,7	41,4	54
5	0,67	1,10	0,62	1,07	31,5	16,6	31,1	-12,7	63
6	0,89	1,46	0,57	0,85	22,7	3,9	27,5	-10,5	72
7	1,15	1,64	0,74	1,22	29,5	19,6	35,9	-4,9	59
8	0,76	1,18	0,65	1,04	29,5	19,9	26,7	8,1	63
9	0,54	1,00	0,45	0,74	31,3	21,7	16,5	-3,2	69
10	0,59	1,03	0,42	0,73	25,9	20,5	26,3	-24,1	59
11	0,64	1,02	0,47	0,85	35,8	39,0	31,0	34,6	55
12	0,60	1,05	0,55	1,05	25,4	7,3	30,4	9,4	71
13	1,02	1,98	0,53	0,85	56,6	14,3	34,7	7,2	61
14	0,79	1,22	0,72	1,12	33,0	-20,6	31,7	-8,9	60
15	0,72	1,11	0,50	0,80	28,2	7,1	37,3	-35,3	63
16	0,59	0,97	0,48	0,73	20,5	10,4	25,0	-10,6	72
17	0,61	1,01	0,58	1,02	34,2	20,3	40,2	36,0	54
18	0,76	1,24	0,49	0,84	19,9	11,6	23,5	6,0	72
19	0,57	0,94	0,35	0,60	24,2	8,4	17,4	14,8	73
20	1,43	2,45	0,48	0,76	35,3	16,6	33,9	44,3	51
21	0,76	1,26	0,54	0,89	31,0	6,2	30,5	33,0	63
22	1,06	2,19	0,69	1,28	25,8	7,7	25,1	-4,9	67
23	0,62	1,03	0,54	0,90	22,6	21,6	33,0	-25,9	56
24	0,84	1,44	0,45	0,73	23,3	11,2	30,6	3,7	72
25	0,62	0,97	0,48	0,81	32,6	21,8	23,5	3,1	68
26	0,86	1,48	0,65	1,04	44,0	47,3	28,7	0,3	63
27	0,68	1,20	0,62	1,03	16,6	6,4	20,6	-14,6	70
28	0,84	1,33	0,53	0,81	34,9	30,6	24,6	-9,4	62
29	1,01	1,55	0,54	0,82	44,3	29,4	29,1	-7,4	60
30	0,77	1,23	0,56	0,88	26,9	23,8	44,2	75,6	53
31	0,70	1,05	0,60	0,93	66,2	-33,0	24,6	-5,9	60
32	0,64	1,06	0,72	1,18	24,9	15,3	22,7	5,8	68
33	0,91	1,45	0,78	1,21	28,1	4,7	41,0	-12,1	65
34	0,78	1,21	0,57	0,98	26,4	24,1	21,2	-3,5	66
35	0,86	1,33	0,66	1,21	36,1	24,3	33,1	-16,7	55
36	0,81	1,24	0,60	0,91	23,5	16,6	27,4	-23,4	58
37	0,80	1,32	0,57	0,87	29,4	16,8	21,1	6,9	67
38	0,63	0,98	0,56	0,90	17,3	-1,9	21,3	-6,5	79
39	0,73	1,15	0,45	0,73	25,1	10,4	19,1	-4,1	75
40	0,83	1,29	0,45	0,74	34,3	-8,1	21,3	2,0	75
Avg	0,77	1,26	0,56	0,92	30,7	13,6	28,1	4,3	64
	$\pm 0,18$	$\pm 0,33$	$\pm 0,10$	$\pm 0,18$	$\pm 9,61$	$\pm 15,00$	$\pm 7,39$	$\pm 23,84$	$\pm 7,46$

Figure 7: Evaluation of automatic segmentations against ground truth for 40 training datasets.

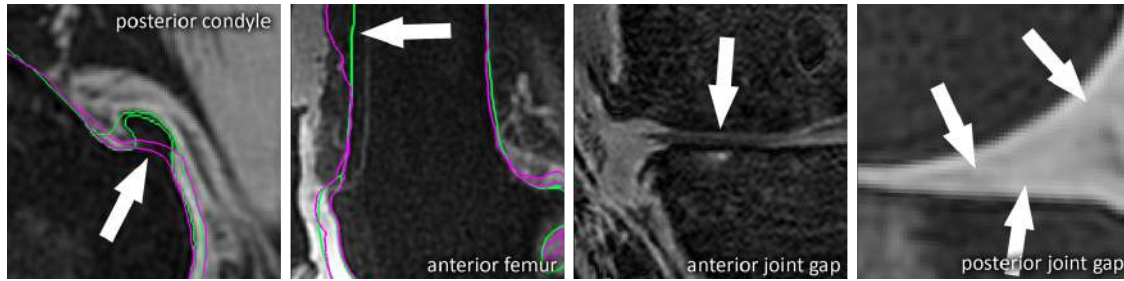


Figure 8: Challenging regions: Large osteophytes with high curvature, Low contrast at anterior bone-shaft to soft-tissue interface, Strong cartilage wear, Low contrast at cartilage to soft-tissue interface, Under-segmented bone at cartilage interface.

3.1.2 Example: 3D reconstruction from X-ray

The orientation of the natural acetabulum is useful for total hip arthroplasty (THA) planning and for researching acetabular problems. Currently the same acetabular component orientation goal is generally applied to all THA patients. Creating a patient-specific plan could improve the clinical outcome. The gold standard for surgical planning is from three-dimensional (3D) computed tomography (CT) imaging. However, this adds time and cost, and exposes the patient to a substantial radiation dose. If the acetabular orientation could be reliably derived from the standard anteroposterior (AP) radiograph, preoperative planning would be more widespread, and research analyses could be applied to retrospective data, after a postoperative issue is discovered. The reduced dimensionality in 2D X-ray images and its perspective distortion, however, lead to ambiguities that render an accurate assessment of the orientation parameters a difficult task. One goal is to enable robust measurement of the acetabular inclination and version on 2D X-rays using computer-aided techniques.

Based on the idea of Lamecker et al. [17], Ehlke et al. [4] propose a reconstruction method to determine the natural acetabular orientation from a single, preoperative X-ray. The basic idea is to

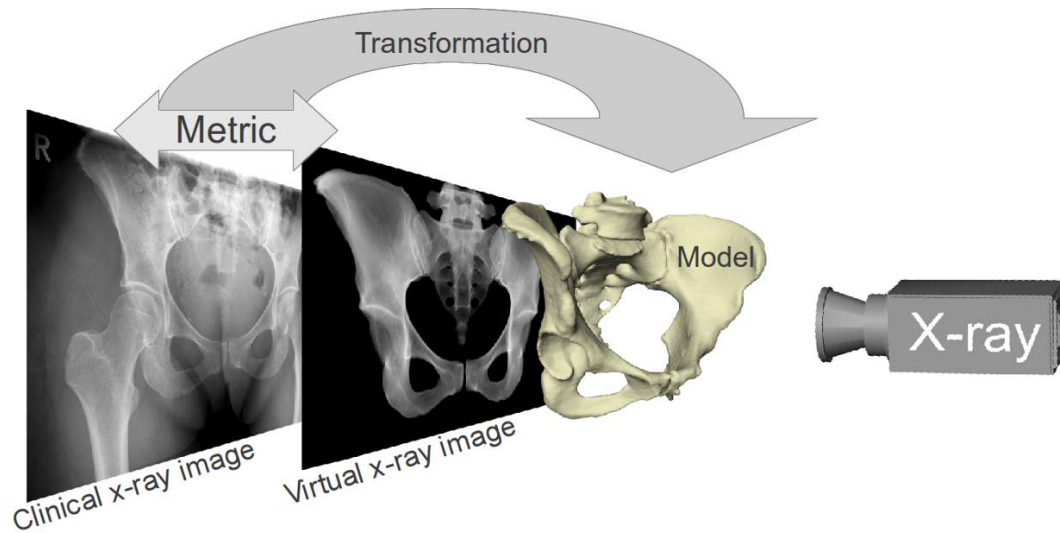


Figure 9: The 3D shape reconstruction process from X-ray images optimizes the similarity between virtual X-ray images generate from the SSIM with the clinical X-ray images.

take virtual X-rays of a (extended) SSM and compare them to a clinical X-ray in an optimization framework. The best matching model instance gives an estimated shape and pose (and bone density distribution) of the subject (Fig. 9). The acetabular orientation (Fig. 10) can then be assessed directly from the reconstructed, patientspecific anatomy model [6, 5]. The approach utilizes novel articulated statistical shape and intensity models (ASSIMs) that express the variance in anatomical shape and bone density of the pelvis/proximal femur between individual patients and model the articulation of the hip joints.

Concerning the application of SSMs to the anatomy of joints and their involved bones, one must also consider the variation of joint posture. A straightforward idea is not to care about joints at all and hence to employ multiple, independent models of the individual bones. However, there are two major drawbacks with this approach: First, an objects pose is independent of its adjacent object(s). This allows arbitrary object poses that do not resemble natural joint postures. Second, the shape

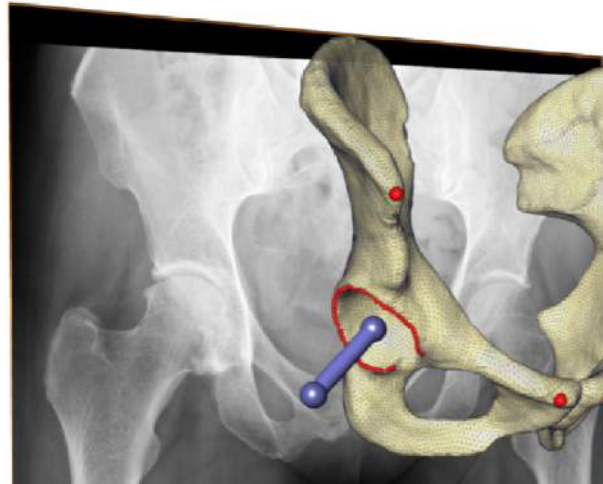


Figure 10: AP radiograph with reconstructed ilia, APP and acetabular reference landmarks (red), and global acetabular orientation vector (blue). Note that the person is standing in front of the Xray plane, and the projection onto the plane is modeled.

of two neighbor bones is decoupled, although the adjacent surfaces of contact may correspond with regard to their shape. To eliminate these shortcomings, Bindernagel et al. [1] propose an articulated SSM (ASSM), which considers degrees of freedom that are better suited to such object compounds, see Fig. 11).

In contrast to previous surface-based methods, the ASSIM-based reconstruction approach not only considers the anatomical shape of the pelvis, but also the bone interior density of both the pelvis and proximal femur. The rationale is to use as much information contained in the X-ray as possible, in order to increase the robustness of the 3D reconstruction (Fig. 12)

A preliminary evaluation on 6 preoperative AP X-ray and matching CT datasets, for the pelvis and femur of 6 different patients, was performed. The patient-specific 3D anatomies were first reconstructed from the 2D images and the inclination and version parameters obtained using the proposed method. These parameters were then compared to gold-standard values assessed inde-

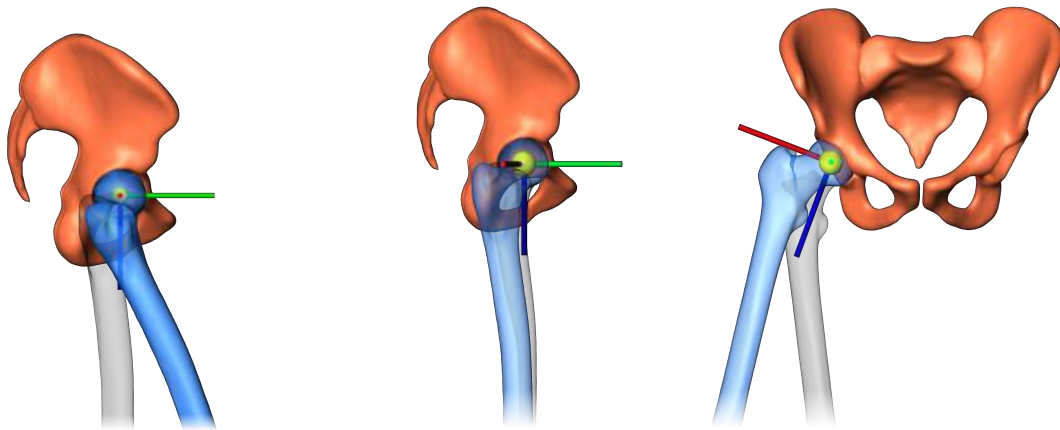


Figure 11: The spheroidal joint model that is used for the hip realizes three consecutive rotations around the depicted axes. Variation of hip joint posture (default pose is outlined in gray): (a) Rotation around x-axis (red), (b) Rotation around z-axis (blue), (c) (c) Rotation around y-axis (green).

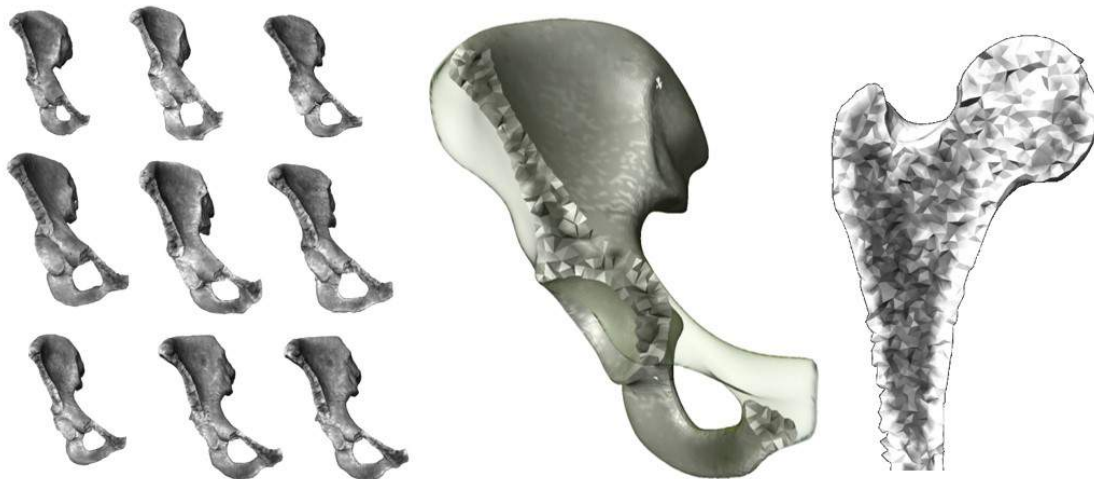


Figure 12: Statistical shape and intensity models also take into account the intensity distribution inside the volume of the anatomical structure.

pendently from the individual patient's CT data. Average acetabular orientation errors, in absolute values, between the 3Dreconstructed values and the CT gold standard for the right/left hips were $3.86^\circ/2.77^\circ$ in inclination and $3.73^\circ/4.97^\circ$ in version. Maximum errors were $8.26^\circ/5.43^\circ$ in inclination and $6.22^\circ/8.27^\circ$ in version.

In most cases, the method produced results close to the CT gold standard (e.g. with an error margin of 4°). For the two outliers with an error above 8° , an incorrect fit between the model and reference X-ray was observable in the respective acetabular region, indicating that the statistical model needs to be enhanced further by expanding the training base. Also, currently the anterior pelvic plane is determined from only 4 points. Using a different plane as reference might increase the robustness when computing the inclination and version parameters.

3.2 Reconstructive Surgery

Surgical treatment is necessary in case of missing or malformed bony structures, e.g. due to congenital diseases, tumors, fractures or malformations arising from osteoarthritis. The task of the surgeon is to restore the patient's bone to resemble its former healthy state as good as possible. This is not an easy task as the former non-pathological state is generally not known. Hence the surgeon has no objective guideline on how to perform the restoration. However, in many cases, some healthy bone in the vicinity of the pathological region remains. The SSM of a complete structure may be fit to that region and used to bridge the pathological region, and thus create an objective, yet individual reconstruction guide.



Figure 13: Three cases of hemifacial microsomia with evidently malformed mandibles.

3.2.1 Example: Mandible dyplasia

Patients with distinct craniofacial deformities or missing bony structures require a surgical reconstruction that in general is a very complex and difficult task. The main reasons for such malformations, as show in Fig. 13, are tumor related bone resections or craniofacial microsomia. In cases where the reconstruction cannot be guided by the symmetry of anatomical structures, it becomes particularly challenging. Then a surgeon must compare the individual pathologic situation with a mental image of a regular anatomy to modify the affected structures accordingly. For such a surgical therapy osteotomies are typically performed with either subsequent osteodistraktion or osteosynthesis after relocation of bony segments, sometimes even in combination with selective bone and soft tissue augmentation. In many cases of mandibular dysplasia and hemifacial microsomia, any kind of guideline for the perception of a designated objective is highly desired.

Zachow et al. [21] propose a method based on a SSM of the mandible bone for reconstructing missing or malformed bony structures. This is achieved by selecting parts of the mandible that are

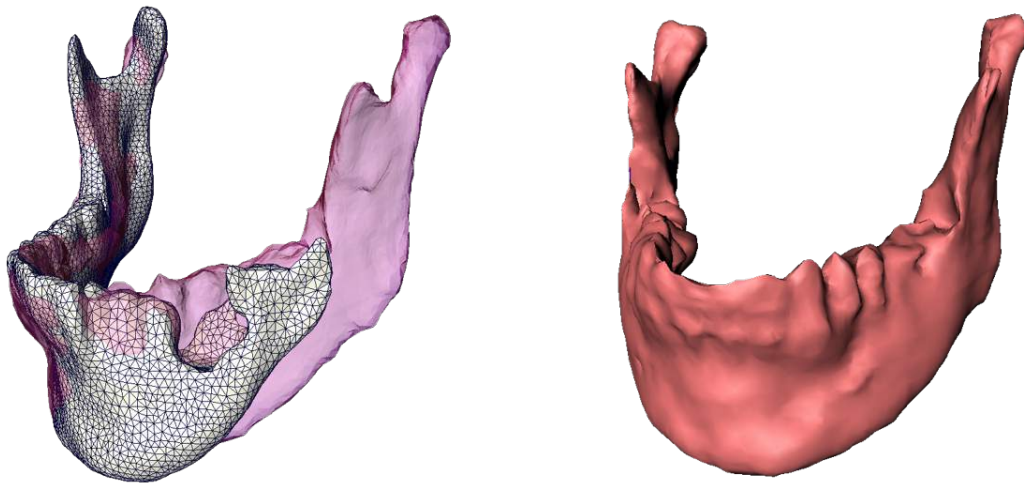


Figure 14: Template generation for patient P1, see table 1: a) hypoplastic mandible, b) mean mandible shape, c) adaptation of the shape model to the right part of the mandible, d) 3D template for mandible reconstruction.

considered as being regularly shaped and therefore are to be preserved.

A statistical 3D shape model of the human mandible seems to be a valuable planning aid for surgical reconstruction of bone defects. This is particularly useful for severe cases of hemifacial microsomia (Fig. 14). With a best matching candidate of the shape model, regarding the size and the shape of available bone, a surgeon gets a good mental perception of the reconstruction that is to be performed.

3.2.2 Example: Craniosynostosis

Premature ossified cranial sutures of infants (craniosynostosis) often lead to skull deformities in the growth process. This can lead to increased intracranial pressure, vision, hearing, and breathing problems. Since research on the correction of underlying disorders on the cellular level is still

being carried on patients with craniosynostosis depend on surgical intervention for preventing or reducing functional impairment and improving their appearance. The most commonly used surgical procedure consists of bone fragmentation, deformation (reshaping) and repositioning. A major problem is the evaluation of the aesthetic results of reshaping the cranial vault in small children as the literature does not provide sufficient criteria for assessing skull shape during infancy. A definition of the correct target shape after surgery is missing. The most important and in many cases only indication of the best possible approximation of the skull shape to the unknown healthy shape is left to the subjective aesthetic assessment of the surgeon. This prevents impartial control of therapeutic success and aggravates guidance and instruction of the remodelling process for inexperienced surgeons.

Lamecker et al. [18] and Hochfeld et al. [12] have developed a statistical 3D-shape model of the upper skull to provide an objective, yet patient-specific guidance for the remodelling. To this end, a statistical 3D-shape model of the upper skull is generated from a set of 21 MRI data sets of healthy infants. The 3D cranial model serves as a template for the reshaping process, by finding an optimal fit of any of its variations to a given malformed skull. Usually, no pre-operative MRI scan is available for the infant patients (mostly under the age of one year) in order to avoid unnecessary anaesthesia. Hence the matching of the model towards the pathological skull of the patient is performed by non-invasively measuring anthropometric distances that are not affected by the surgical intervention:

- width between both entries of the auditory canals
- distance from nasion to occiput
- height between vertex and the midpoint of the line between the auditory canals

These distances are extrapolated to the skull surface by approximating the skin and skull thickness. The shape model instance that best fits these measurements is selected as a template for the reconstruction process. The resulting shape instance represents an individual interpolation of all shapes contained in the training set.

In a first clinical application, the statistical model was pre-operatively matched to a patient using the method described above. From this computed shape model instance a life-size facsimile of the skull was built and taken to the operating room to guide the reshaping process. Fig. 15 illustrate the surgical procedure and the role of the statistical skull model.

3.2.3 Example: Surgical Reconstruction of Complex Fractures in the Midface

Surgical interventions on the craniofacial bone in cases of complex defects spanning the facial mid-plane (e.g. horse kick fractures) require high precision during planning as well intra-operatively (Fig. 16, left). The goal is to restore function but also create aesthetically appealing reconstructions of the fractured parts. Mirroring of the intact side is often not possible. If there no pre-traumatic tomographic data of the anatomical region of the patient is available the re-location of the bone fragments is performed according to the subjective perception and personal skill of the operator.

In order to overcome this situation and possibly restore (or even improve) the pre-traumatic situation an objective guideline for the surgical procedure is desirable. Several central questions need to addressed: (1) What is an objective guideline for re-modeling the bony structures of the midface? (2) How may the surgeon be supplied with a practical tool to perform the reconstruction based on the planning data? (3) Can the planning guideline be generated fast enough such that it may be used immediately in a first emergency operation?

Zachow et al. [22] propose a way to tackle those challenges based on SSMs. In their work, a



(a) Three different views of a patient with trigonocephaly (ossification of the suture running down the midline of the forehead) - before surgery.



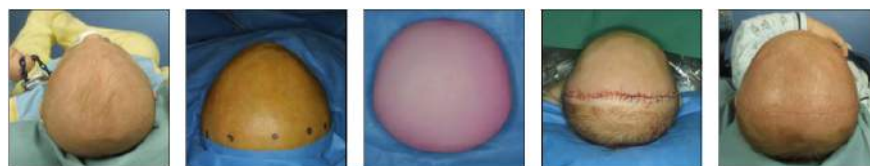
(b) Cutting lines indicated on the skull, removed frontal skull region before the reshaping, facsimile of shape model instance on which bone parts are reshaped.



(c) Bone stripe before and after reshaping, result of reshaping process on model.



(d) Microplates for fixating bone pieces on remaining skull are also shaped on the model, result after fixation of reshaped bone on skull.



(e) Comparison between pre- and post-operative situation (from left to right): patient 2 months before surgery, immediately before surgery, fac-simile of the target shape derived from the statistical model, patient immediately after surgery, 3 weeks after surgery.

Figure 15: Craniosynostosis surgery based on a SSM.

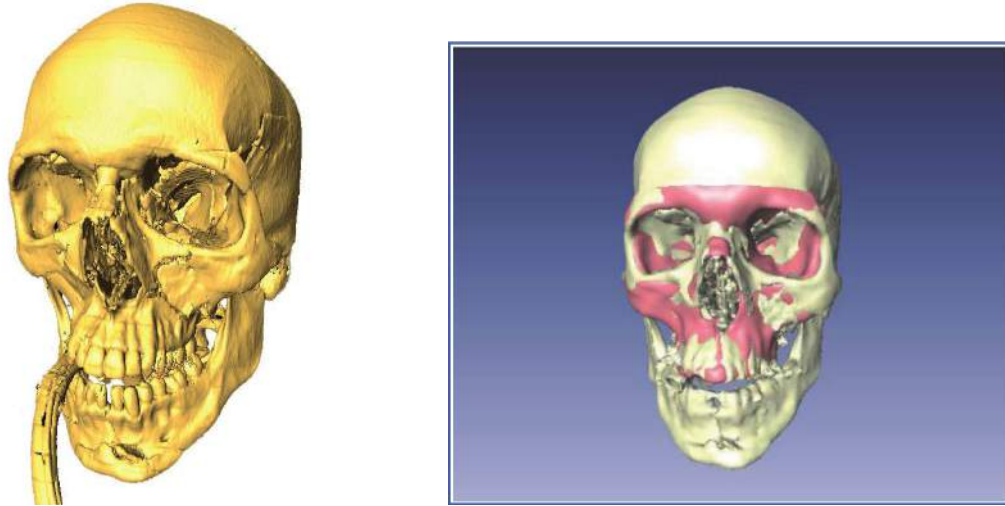


Figure 16: Left: Midface trauma visualized by an isosurface of the CT data. Right: Reconstruction proposal based on a SSM (red).

SSM representing normal bone anatomy is used to segment a CT data set of a traumatic patient. Fractured regions in the image are masked so they are ignored in the fitting process. The resulting SSM then interpolates those regions thereby creating a “normal” shape guideline in those regions, which matches the patient’s anatomy in healthy regions (Fig. 16, right). This computation takes only several minutes on standard computers.

In order to transfer the plan to the intra-operative situation the reconstructed geometry can rasterized to the grid of the CT data and exported in DICOM format directly to the navigation system. There, it can be presented to the surgeon as an overlay on the CT data. The surgeon can mobilize bone fragments towards the targeted position on the SSM, and there perform the osteosynthesis (Fig. 17).

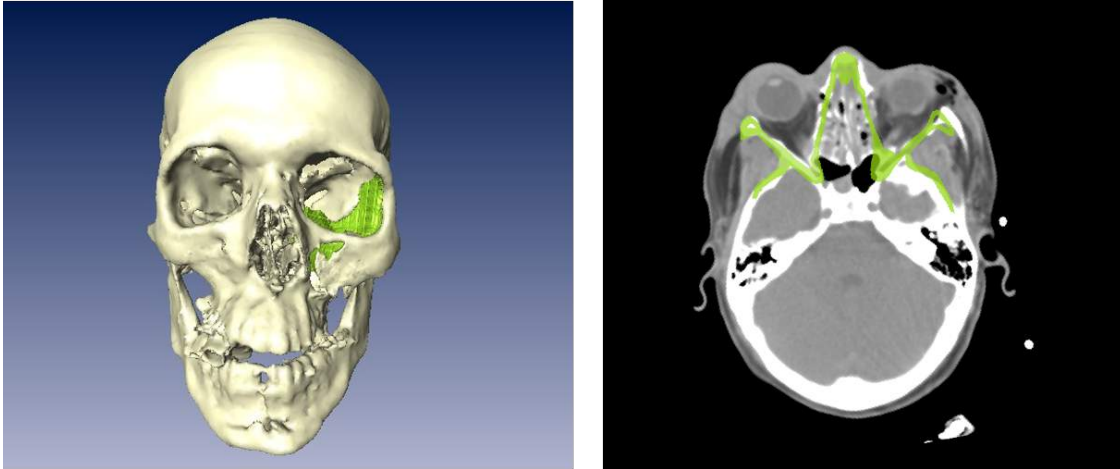


Figure 17: Left: 3D visualization of deviation of fractured bone (white) to targeted SSM-based planning (green). Right: Overlay of planning result in DICOM data.

3.3 Population-based Analysis

SSMs represent the shape variability contained in a specific population with few degrees of freedom. Furthermore, they are based on a common parameterization of the shapes. This means that computationally demanding analyses (local, regional or global), such as finite-element studies, across subjects can be performed efficiently. Parameter studies or inverse problems become more tractable due to the compact representation of shape and the small number of shape parameters. This allows to study, e.g. the relationship between shape and socio-demographic or biomechanical parameters (e.g. fracture risk). Instead of performing fully individualized procedures implant design or procedures may be optimized based on population studies, see e.g. [15].

3.3.1 Example: A large scale finite element study of total knee replacements

The aim of the study performed by Galloway et al. [7] is to investigate the performance of a cementless osseointegrated tibial tray (P.F.C. Sigmas, Depuy Inc., USA) in a general population using

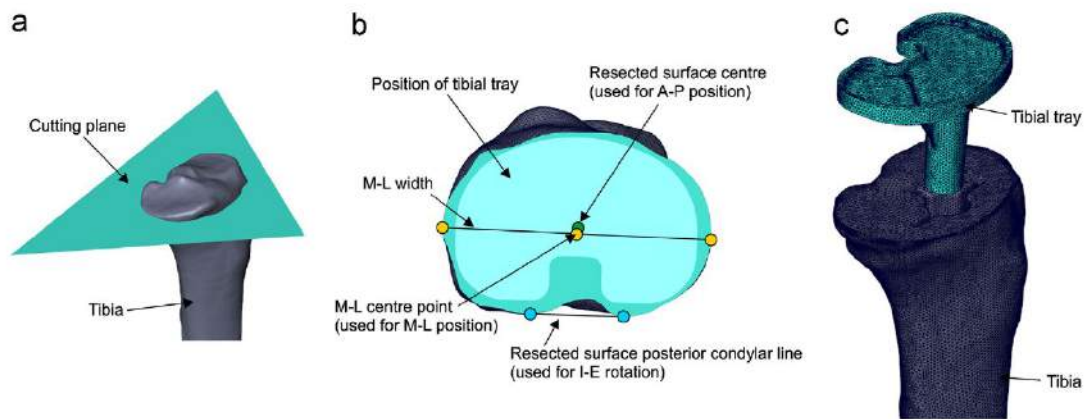


Figure 18: Selected steps of implanting the tibial tray: (a) shows the position of the cutting plane, (b) shows the landmarks used on the resected surface to position the tibial tray, and (c) is an exploded view of mesh components (Tetra).

finite element (FE) analysis. Computational testing of total knee replacements (TKRs) typically only use a model of a single patient and assume the results can be extrapolated to the general population. In this study, two SSMs were used; one of the shape and elastic modulus of the tibia, and one of the tibiofemoral joint loads over a gait cycle, to generate a population of FE models. A method was developed to automatically size, position and implant the tibial tray in each tibia, and 328 models were successfully implanted and analyzed, see Fig. 18.

The composite peak strain (CPS) during the complete gait cycle in the bone of the resected surface was examined and the “percentage surface area of bone above yield strain” (PSAY) was used to determine the risk of failure of a model. Using an arbitrary threshold of 10% PSAY, the models were divided into two groups (“higher risk” and “lower risk”) in order to explore factors that may influence potential failure. In this study, 17% of models were in the “higher risk” group and it was found that these models had a lower elastic modulus (mean 275.7 MPa), a higher weight (mean 85.3 kg), and larger peak loads, of which the axial force was the most significant. This study

showed the mean peak strain of the resected surface and PSAY were not significantly different between implant sizes.

It was observed that the distribution of the CPS changed as the PSAY increased. For models with a low PSAY (e.g. “lower risk” case Fig. 19), higher strains were seen around the anterior and posterior edges. As the PSAY increases, models around the 10% threshold (e.g. “border case” Fig. 19) tended to have bone above yield strain around the periphery. The strains on the lateral side tended to be higher in comparison to the medial side. In the “higher risk” group, bone above yield tended to be distributed over the whole resected surface (e.g. “higher risk” case Fig. 19), although in some cases only the lateral side was above yield. The pattern of strain is most likely due to the difference in modulus between the lateral and medial side of the resection surface.

3.3.2 Example: Digital Morphometry of Facial Anatomy, From Global to Local Shape Variations

Although the following example is not directly related to orthopedic interventions it illustrates the potential of SSMs for population analysis in order to examine clusters or systematic variation related to covariates, such as demographic factors or pathology indicators.

Facial proportions largely depend on maturation (age) and sex. Maturation increases the proportion facial height to head height, the eyes tend to become narrower, and the bigonial to bizygomatic proportions enlarges. Proportions that associate with sex, involve structures close to nose and cheek. Only 25% of the variance of facial proportions, mainly those describing variation in the lower and in the mid-face, are independent of sex and age, but are often affected in dysmorphic syndromes [11]. Grewe et al. [9] investigate 52 North German child and adolescent faces aged 2 to 23 years (26 male, 26 female) acquired with a 3D laser scanner [8]. Based on a mesh with 10,000

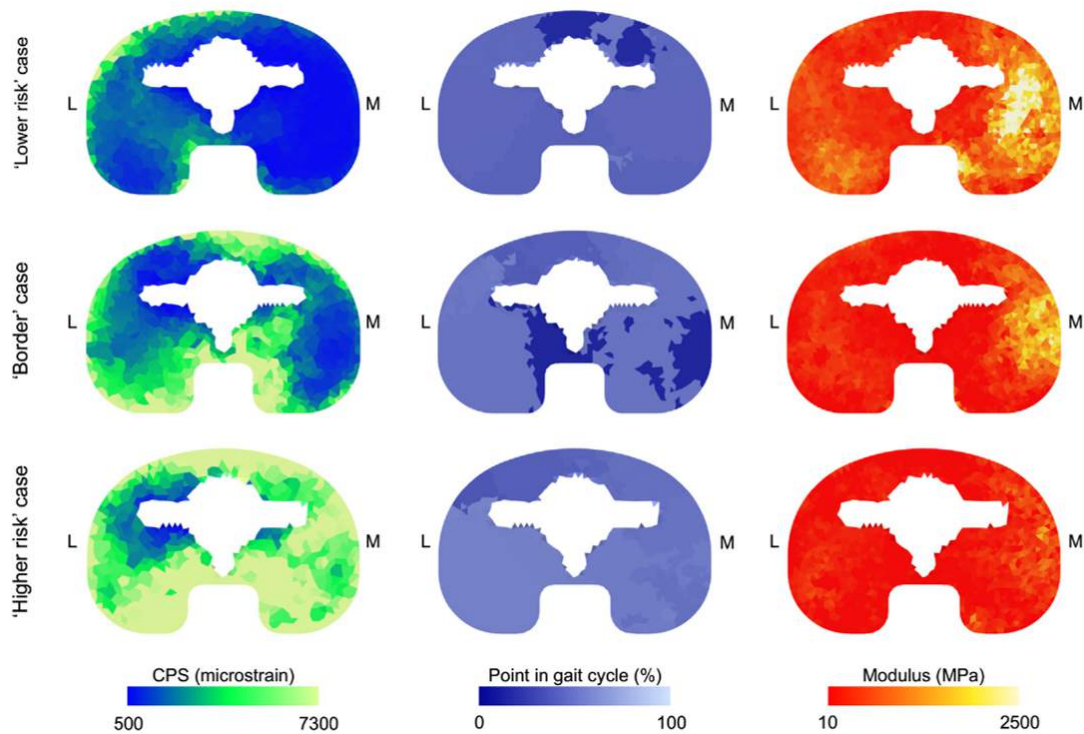


Figure 19: Three example cases of the resected surface. Top is a “lower risk” case (PSAY=1.45%), middle is a “border” case (PSAY=9.05%), and bottom is a “higher risk” case (PSAY=39.75%). Each is plotted with the CPS (left), the point in the gait cycle at which the peak strain occurs (middle), and modulus(right).

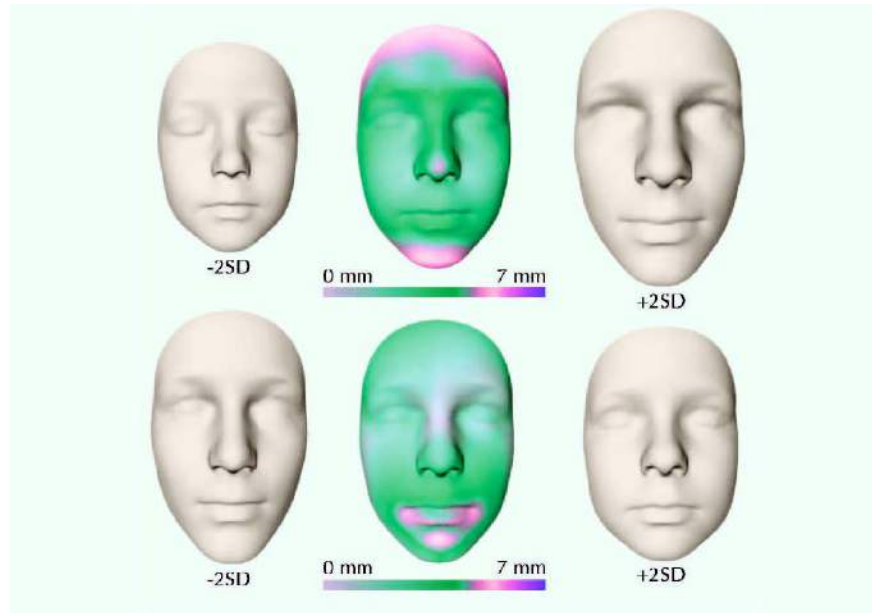


Figure 20: The first two parameters of the face SSM. Middle column: shape variation color-coded on the average face. Left/Right column: face instances when varying the parameter by $-2/+2$ standard deviations.

points a SSM was created.

Visualization techniques can be employed to explore the nature of the shape model parameters as well as the distribution of the data set. Fig. 20 shows that PCA parameters in general have a global effect on the shape, i.e. the shape variation is spread over a large portion of the anatomical region. Sometimes region-specific parameters e.g. for eyes, mouth or nose are desirable. A special class of orthogonal transformations, known as VARIMAX rotations [14], lead to parameters with locally concentrated variation, thus yielding meaningful parameters, e.g. for changing the shape of the nose (Fig. 21). This can be used to synthesize new shapes more intuitively.

Shape variation was also regressed on sex and age. Fig. 22 shows shape instances computed via the regression function for sex specific shape variation for age. Such information may, for instance, be useful for forensic purposes.

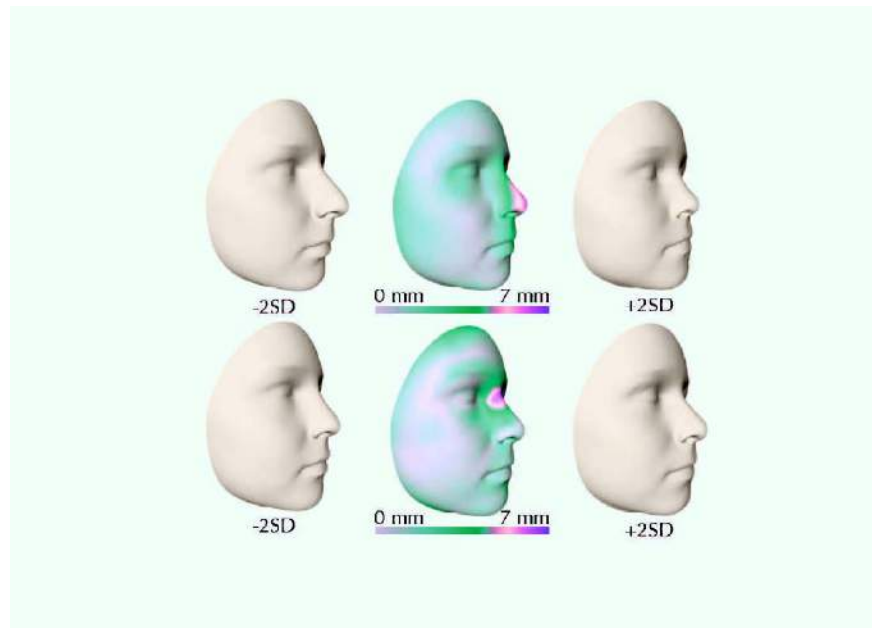


Figure 21: Varimax transformed SSM with meaningful parameters for changing the shape of the nose.

Columns as in Fig. 20.

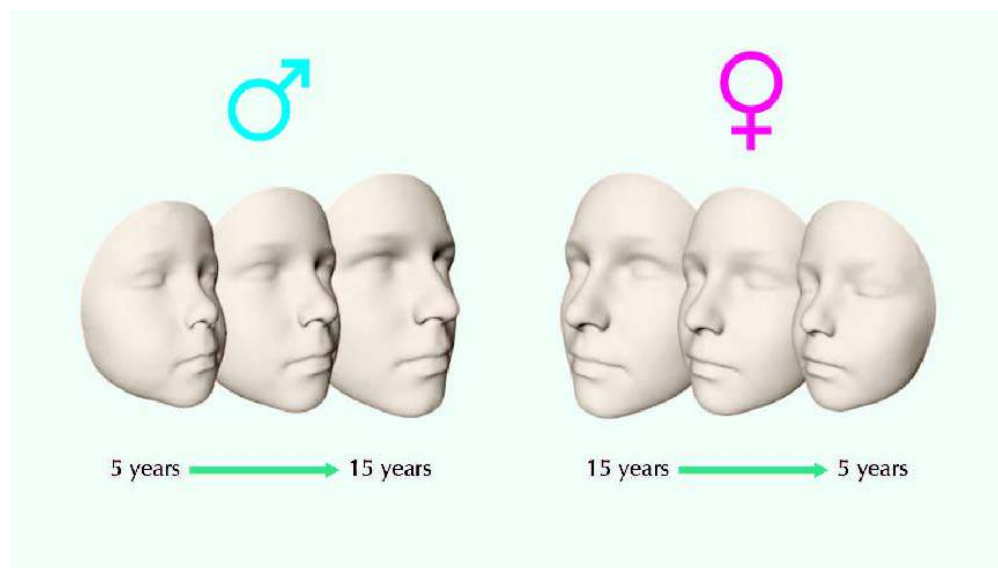


Figure 22: Sex specific ageing time line produced by the regression function (5, 10, 15 years).

4 Conclusions

In this chapter we have described the concept of statistical shape models. We have illustrated that this technology has a major impact in three different fields:

1. Reconstruction of anatomical structures from medical images, both 3D (CT or MRI) and 2D (X-ray) data.
2. Planning of complex surgical interventions and the use of such plans intra-operatively.
3. Population analysis to gain a deeper understanding about how shape or shape changes are related to external parameters such as biomechanical, demographic or clinical factors.

One reason for the usefulness of SSMs are their power to reduce the complexity of shape representation. A SSM is able to describe shape variations contained in a population with few degrees of freedom. This allows to synthesize or reconstruct new shapes even based on noisy or partial data, usually in an efficient manner.

The full potential of SSMs still remains to be unleashed. On the one hand, the combination of several individual objects into compounds remains a big challenge. On the other hand, with increasing number of imaging modalities and sources, concepts that combine shape information on different scales would offer new possibilities. Furthermore, on a more fundamental level, the correspondence identification process will remain a field of active research, even more so when higher details can be captured by such models.

References

- [1] M. Bindernagel, D. Kainmueller, H. Seim, H. Lamecker, S. Zachow, and H.-C. Hege. An articulated statistical shape model of the human knee. In *Bildverarbeitung für die Medizin 2011*, pages 59 – 63, 2011. doi: 10.1007/978-3-642-19335-4_14.
- [2] T. F. Cootes, C. J. Taylor, D. H. Cooper, and J. Graham. Active shape models—their training and application. *Comput. Vis. Image Underst.*, 61(1):38–59, Jan. 1995. ISSN 1077-3142. doi: 10.1006/cviu.1995.1004. URL <http://dx.doi.org/10.1006/cviu.1995.1004>.
- [3] R. Davies, C. Twining, T. Cootes, J. Waterton, and C. Taylor. A minimum description length approach to statistical shape modeling. *Medical Imaging, IEEE Transactions on*, 21(5):525–537, May 2002. ISSN 0278-0062. doi: 10.1109/TMI.2002.1009388.
- [4] M. Ehlke, H. Ramm, H. Lamecker, H.-C. Hege, and S. Zachow. Fast generation of virtual x-ray images for reconstruction of 3d anatomy. *IEEE Transactions on Visualization and Computer Graphics*, 19(12):2673 – 2682, 2013. doi: 10.1109/TVCG.2013.159.
- [5] M. Ehlke, T. Frenzel, H. Ramm, H. Lamecker, M. A. Shandiz, C. Anglin, and S. Zachow. Robust measurement of natural acetabular orientation from ap radiographs using articulated 3d shape and intensity models. Technical Report 14-12, ZIB, Takustr.7, 14195 Berlin, 2014.
- [6] M. Ehlke, T. Frenzel, H. Ramm, M. A. Shandiz, C. Anglin, and S. Zachow. Towards robust measurement of pelvic parameters from ap radiographs using articulated 3d models. In *Computer Assisted Radiology and Surgery (CARS)*, 2015. accepted for publication.

- [7] F. Galloway, M. Kahnt, H. Ramm, P. Worsley, S. Zachow, P. Nair, and M. Taylor. A large scale finite element study of a cementless osseointegrated tibial tray. *Journal of Biomechanics*, 46(11):1900 – 1906, 2013. doi: /10.1016/j.jbiomech.2013.04.021.
- [8] C. M. Grewe, H. Lamecker, and S. Zachow. Digital morphometry: The potential of statistical shape models, 2011.
- [9] C. M. Grewe, H. Lamecker, and S. Zachow. Landmark-based statistical shape analysis. In M. Hermanussen, editor, *Auxology - Studying Human Growth and Development url*, pages 199 – 201. Schweizerbart Science Publishers, 2013. URL <http://www.schweizerbart.de/publications/detail/isbn/9783510652785>.
- [10] T. Heimann and H.-P. Meinzer. Statistical shape models for 3d medical image segmentation: A review. *Medical Image Analysis*, 13(4):543 – 563, 2009. ISSN 1361-8415. doi: <http://dx.doi.org/10.1016/j.media.2009.05.004>. URL <http://www.sciencedirect.com/science/article/pii/S1361841509000425>.
- [11] E. M. Hermanussen, editor. *Auxology*. Schweizerbart Science Publishers, Stuttgart, Germany, 03 2013. ISBN 9783510652785. URL http://www.schweizerbart.de//publications/detail/isbn/9783510652785/Hermanussen_Auxology.
- [12] M. Hochfeld, H. Lamecker, U. W. Thomale, M. Schulz, S. Zachow, and H. Haberl. Frame-based cranial reconstruction. *Journal of Neurosurgery: Pediatrics*, 13(3):319 – 323, 2014. doi: 10.3171/2013.11.PEDS1369.
- [13] D. Kainmüller, H. Lamecker, M. Heller, B. Weber, H.-C. Hege, and S. Zachow. Omnidi-

- rectional displacements for deformable surfaces. *Medical Image Analysis*, 17(4):429 – 441, 2013. doi: 10.1016/j.media.2012.11.006.
- [14] H. Kaiser. The varimax criterion for analytic rotation in factor analysis. *Psychometrika*, 23(3):187–200, 1958. ISSN 0033-3123. doi: 10.1007/BF02289233. URL <http://dx.doi.org/10.1007/BF02289233>.
- [15] N. Kozic, S. Weber, P. Bchler, C. Lutz, N. Reimers, M. . G. Ballester, and M. Reyes. Optimisation of orthopaedic implant design using statistical shape space analysis based on level sets. *Medical Image Analysis*, 14(3):265 – 275, 2010. ISSN 1361-8415. doi: <http://dx.doi.org/10.1016/j.media.2010.02.008>. URL <http://www.sciencedirect.com/science/article/pii/S136184151000023X>.
- [16] H. Lamecker. *Variational and statistical shape modeling for 3D geometry reconstruction*. PhD thesis, Freie Universit”at Berlin, 2009.
- [17] H. Lamecker, T. Wenckeback, and H.-C. Hege. Atlas-based 3d-shape reconstruction from x-ray images. In *Proc. Int. Conf. of Pattern Recognition (ICPR2006)*, volume Volume I, pages 371 – 374, 2006. doi: 10.1109/ICPR.2006.279.
- [18] H. Lamecker, S. Zachow, H.-C. Hege, and M. Zöckler. Surgical treatment of craniosynostosis based on a statistical 3d-shape model. *Int. J. Computer Assisted Radiology and Surgery*, 1(1): 253 – 254, 2006. doi: 10.1007/s11548-006-0024-x.
- [19] N. Sarkalkan, H. Weinans, and A. A. Zadpoor. Statistical shape and appearance models of bones. *Bone*, 60(0):129 – 140, 2014. ISSN 8756-3282. doi: <http://dx.doi.org/>

10.1016/j.bone.2013.12.006. URL <http://www.sciencedirect.com/science/article/pii/S8756328213004948>.

- [20] H. Seim, D. Kainmueller, H. Lamecker, M. Bindernagel, J. Malinowski, and S. Zachow. Model-based auto-segmentation of knee bones and cartilage in mri data. In B. v. Ginneken, editor, *Proc. MICCAI Workshop Medical Image Analysis for the Clinic*, pages 215 – 223, 2010.
- [21] S. Zachow, H. Lamecker, B. Elsholtz, and M. Stiller. Reconstruction of mandibular dysplasia using a statistical 3d shape model. In *Proc. Computer Assisted Radiology and Surgery (CARS)*, pages 1238 – 1243, 2005. doi: 10.1016/j.ics.2005.03.339.
- [22] S. Zachow, K. Kubiack, J. Malinowski, H. Lamecker, H. Essig, and N.-C. Gellrich. Modellgestützte chirurgische rekonstruktion komplexer mittelgesichtsfrakturen. In *Proc. BMT, Biomed Tech 2010*, volume 55 (Suppl 1), pages 107 – 108, 2010.